Contribution of the Na^+/Ca^{2+} Exchanger to Rapid Ca^{2+} Release in Cardiomyocytes

Glenn T. Lines,* Jørn B. Sande,*† William E. Louch,† Halvor K. Mørk,† Per Grøttum,‡ and Ole M. Sejersted†
*Simula Research Laboratory, Lysaker, Norway; and †Institute for Experimental Medical Research, Ullevaal University Hospital and Center for Heart Failure Research, and ‡Section of Medical Informatics, University of Oslo, Oslo, Norway

ABSTRACT Trigger Ca^{2+} is considered to be the Ca^{2+} current through the L-type Ca^{2+} channel (LTCC) that causes release of Ca^{2+} from the sarcoplasmic reticulum. However, cell contraction also occurs in the absence of the LTCC current (I_{Ca}). In this article, we investigate the contribution of the Na^+/Ca^{2+} exchanger (NCX) to the trigger Ca^{2+}. Experimental data from rat cardiomyocytes using confocal microscopy indicating that inhibition of reverse mode Na^+/Ca^{2+} exchange delays the Ca^{2+} transient by 3–4 ms served as a basis for the mathematical model. A detailed computational model of the dyadic cleft (fuzzy space) is presented where the diffusion of both Na^+ and Ca^{2+} is taken into account. Ionic channels are included at discrete locations, making it possible to study the effect of channel position and colocalization. The simulations indicate that if a Na^+ channel is present in the fuzzy space, the NCX is able to bring enough Ca^{2+} into the cell to affect the timing of release. However, this critically depends on channel placement and local diffusion properties. With fuzzy space diffusion in the order of four orders of magnitude lower than in water, triggering through LTCC alone was up to 5 ms slower than with the presence of a Na^+ channel and NCX.

INTRODUCTION

Depolarization of cardiac myocytes during the action potential elicits release of Ca^{2+} from the sarcoplasmic reticulum (SR), which, in turn triggers contraction. Coupling of depolarization to SR Ca^{2+} release occurs in structures called dyads. In the dyads, T-tubules and terminal cisternae of the SR meet in junctional patches where the two membranes are separated by a cleft of ~15 nm. The small subsarcolemmal fluid compartment in the dyadic cleft has also been coined ''fuzzy space'' (1,2). Here Ca^{2+} must diffuse from the inner mouth of the L-type Ca^{2+} channels (LTCC) that open during depolarization of the T-tubular membrane, to reach the ryanodine receptors (RyR) of the SR on the other side of the cleft. Binding of this ''trigger Ca^{2+}'' to RyR initiates Ca^{2+} release from the SR. This is the classical concept of Ca^{2+}-induced Ca^{2+} release (CICR). The process is self-amplifying, but due to restricted diffusion, Ca^{2+} release is limited to a local spark comprising a small number of ryanodine receptors (3). It is the sum of sparks that constitutes the Ca^{2+} transient, and the size of the Ca^{2+} current (number of channels that open) that determines the size of the transient.

This picture of the dyadic cleft and CICR is complicated by the presence of several other membrane proteins, including the Na^+/Ca^{2+} exchanger (NCX). It has recently become clear that although the NCX proteins can be found throughout the sarcolemma, some NCX proteins are localized as close to the RyR as are the LTCCs (4). This raises the question of how the presence of NCX modifies the Ca^{2+} signal in the fuzzy space. The NCX can operate in both a normal forward mode and a reverse mode. Three Na^+ ions are transported in exchange for one Ca^{2+} ion, so that in forward mode the current (I_{NCX}) will be inward, and Ca^{2+} will be pumped out of the cell. A rapid rise of Ca^{2+} in the fuzzy space can therefore be effectively ''buffered'' by the NCX (5). On the other hand, during an action potential, the combination of depolarization and accumulation of Na^+ near the membrane will favor reversal of the NCX. It has been a longstanding question whether reverse mode NCX can contribute to CICR (6–9). Interestingly, cardiac-specific knockout of NCX1 only leads to a small decline of cardiac contractility (10), and overexpression has little effect unless it is substantial when it leads to hypertrophy and myocardial failure (11). Hence it seems clear that in species with a high reliance on SR for the Ca^{2+} transient, NCX predominantly plays a modulatory role for the $[Ca^{2+}]_i$ in the dyadic cleft.

This article focuses on the potential role of NCX in triggering Ca^{2+} release. There are reports that in the absence of an L-type Ca^{2+} current (I_{Ca}), close to normal contractions can be triggered by reverse mode exchange (12,8,13,7). However, recent experiments indicate that conditions for reverse mode exchange may have disappeared as soon as 5 ms after rapid depolarization and that accumulation of Ca^{2+} in the cleft rapidly switches the exchanger into forward transport mode (14,15). After 5 ms, some repolarization has occurred during a normal action potential and local accumulation of Na^+ might already be dissipated. Several investigators have modeled the events that take place in the dyadic cleft treating the fuzzy space as one compartment (16–20). However, it is clear that there is a diffusion distance, and it has been argued that diffusion is slow in this fuzzy space. This makes it necessary to take both number and localization of individual channels and transporters into account.

Submitted August 11, 2005, and accepted for publication April 21, 2006.
Address reprint requests to G. T. Lines, E-mail:glennli@simula.no.

0006-3495/06/08/779/14 $2.00
doi: 10.1529/biophysj.105.072447

The aim of this study was therefore to examine the role of NCX in the very early events of CICR both experimentally and by mathematical modeling. A diffusion model was developed for the dyadic cleft. Specifically, we examine the conditions required for NCX to modify the trigger Ca^{2+} in the dyadic cleft. The results indicate that reverse mode Na^+/Ca^{2+} exchange can precede I_{Ca}, contributing to an early rise of the trigger Ca^{2+}, an effect that subsides after a few milliseconds. The contribution of NCX to the trigger Ca^{2+} depends on two conditions that will require experimental verification. First, diffusion in the fuzzy space must be several orders of magnitude slower than in water, and second, a Na^+ channel must be present within the dyad.

MATERIALS AND METHODS

Animals and cardiomyocyte isolation

Animals were cared for according to the Norwegian Animal Welfare Act, which closely conforms to National Institutes of Health (NIH) guidelines (NIH publication No 85.23, revised 1996). Two animals were kept in each cage and housed in a temperature-regulated room with a 12 h day/12 h night cycling.

Male Wistar rats (Mollegaard Breeding and Research Centre, Skensved, Denmark) weighing ~400 g were intubated and ventilated on a Zoovent ventilator (Triumph Technical Services, Milton Keynes, UK) with 68% N_2O, 29% O_2, and 2–3% Isofluran (Abbott Laboratories, Abbott Park, IL). After injection of heparin i.v., hearts were quickly excised and placed in cold buffer-1 containing (in mM) 130 NaCl, 25 HEPES, 22 D-glucose, 5.4 KCl, 0.5 $MgCl_2$, 0.4 NaH_2PO_4, and 0.01 μg/ml insulin (pH 7.4). Hearts were then cannulated, mounted on a Langendorff setup, and perfused retrogradely (15–25 min) through the aorta with buffer-1 containing 200 U/ml collagenase Type-II and 0.1 mM Ca^{2+}. Left ventricular free wall and septum were minced and gently shaken at 37°C for 3–4 min in the same solution plus 1% bovine serum albumin, 0.02 U/ml deoxyribonuclease I (Worthington Biochemical, Lakewood, NJ). After filtration (200 μm nylon mesh) and sedimentation, the cell pellet was washed three times in buffer-1 (1% bovine serum albumin) with progressively increasing $[Ca^{2+}]$ (0.1, 0.2, 0.5 mM). Isolated cardiomyocytes were stored at room temperature until use.

Experimental protocols

For all experiments, myocytes were loaded with 20 μM Fluo-4 AM (Molecular Probes, Eugene, OR). After 30 min of loading with dye, myocytes were plated on laminin-coated coverslips in a perfusion chamber mounted on the stage of an inverted microscope. When myocytes had adhered, they were superfused at 37°C with HEPES Tyrode solution containing (in mM) 140 NaCl, 1,8 $CaCl_2$, 0.5 $MgCl_2$, 5.0 HEPES, 5.5 glucose, 0.4 NaH_2PO_4, and 5.4 KCl, with pH adjusted to 7.4.

Whole-cell patch clamp experiments were conducted using 1–2 MΩ pipettes. The pipette solution contained (in mM) 120 K-aspartate, 0.5 $MgCl_2$, 6 NaCl, 0.06 EGTA, 10 HEPES, 10 Glucose, 25 KCl, and 4 K_2-ATP. Membrane potential and current recordings were made with an Axoclamp 2B amplifier (Axon Instruments, Foster City, CA) and pCLAMP software (Axon Instruments). $[Ca^{2+}]_i$ transients were elicited at 1 Hz by action potentials or voltage-clamp steps. Action potentials were elicited in bridge-mode using a 3 ms depolarizing current, ~20% above threshold. Discontinuous voltage clamp (sample rate 8 KHz) was used to elicit 100 ms voltage steps to 0 mV from the holding potential of −80 mV. In some experiments, myocytes were field-stimulated through a pair of platinum electrodes with a voltage 50% above threshold.

$[Ca^{2+}]_i$ transients were detected by confocal fluorescence imaging using an LSM 510 scanning system (Zeiss GmbH, Jena, Germany) with a 40× water immersion objective. Fluo-4 was excited at 488 nm, and emission intensity was measured at 510 nm. Myocytes were scanned along the longitudinal axis with a 512-pixel line, every 1.5 ms. Sequential scans were stacked to create two-dimensional images with time in the x axis.

Recordings in control conditions were collected for 1 min. Cells were treated with 5 μM KB-R7942 (KBR) (Tocris/Bio Nuclear AB, Bromma, Sweden), 200 nM tetrodoxin (TTX) (Alomone Labs, Jerusalem, Israel), 5 μM nifedipine (Sigma-Aldrich, St. Louis, MO), or a combination of KBR and TTX.

Data analysis

Image analysis was performed with Scion Image (Scion, Frederick, Maryland), ImageJ (NIH), and SigmaPlot (Jandel Scientific, Northampton, MA) software. Measurements were averaged for three consecutive transients. Data are presented as mean ± SE, and groups were compared statistically with paired or unpaired t-tests. Number of cells is given as n.

Mathematical formulation

The governing law for a diffusing substance P can be derived from mass conservation and Fick's law. It states that

$$\frac{\partial [P]}{\partial t} = \nabla \cdot k_P \nabla P + f,\ x \in \Omega$$
$$k_P \frac{\partial [P]}{\partial t} = J,\ x \in \Gamma, \qquad (1)$$

where ∇P is the gradient of P, and n is a normal vector, i.e., perpendicular to the boundary. Furthermore, Ω is the interior of the domain under consideration, Γ is the boundary of the domain, k_P is the diffusion coefficient for the substance in the fluid, and f represents a source or a drain of the substance. The flow across the boundary is given by J.

Since the focus of this article was the role of the Na^+/Ca^{2+} exchanger, it was important that both Na^+ and Ca^{2+} concentrations were modeled accurately. Consequently, the model in Eq. 1 is used for both of these ions. The equation for the Na^+ concentration is the simplest since there is no internal sources, i.e., f is zero in Eq. 1. The situation is more complicated for Ca^{2+} since the Ca^{2+} buffers act as both drains and sources. Two types of buffers were included, troponin and calmodulin.

The domain Ω will in our case be an area consisting of the fuzzy space between a T-tubule and an SR unit together with some of the surrounding cytosol. The boundary Γ will then consist of the membrane of the T-tubule, the membrane of SR, and artificial boundaries in the cytosol, arising from the mathematical model.

The flux of ions across the membrane was included as boundary conditions. Only the most relevant transmembrane ionic transporters were included. For Na^+, we included the fast inward current I_{Na}, the Na^+/K^+ pump current I_{NaK}, and the Na^+/Ca^{2+} current I_{NCX}. For Ca^{2+}, the included currents were the L-type current I_{Ca} and the Na^+/Ca^{2+} current I_{NCX}. The conversion from current to flux is explained in Eq. 4. The release current from SR, I_{rel}, was not included since we only studied the process leading up to CICR, but not CICR itself.

The membrane currents do not only depend upon the ion concentrations but also on the transmembrane potential and the state of the gating proteins. To compute these currents, we used the model of Winslow et al. (16), which is a set of ordinary differential equations (ODEs). In addition, the Winslow model was changed according to Weber et al. (15) by including an allosteric NCX for activation by Ca^{2+} with $k_{05} = 152$ nM.

For notational convenience, we define $c = [Ca^{2+}]_i$ and $s = [Na^+]_i$. The state variables of the ODE model were lumped together in a vector denoted w. This includes the transmembrane potential, the gating variables, and different ionic concentrations, excluding intracellular Ca^{2+} and Na^+, which were modeled separately. The complete model can be written as

$$\frac{\partial c}{\partial t} = \nabla \cdot k_c \nabla c - I_{BUFFER}(c, w),\ x \in \Omega \qquad (2)$$

$$\frac{\partial s}{\partial t} = \nabla \cdot k_c \nabla s,\ x \in \Omega \tag{3}$$

$$\frac{\partial c}{\partial t} = F(w, \bar{s}_B, \bar{c}_B, \bar{c}_F). \tag{4}$$

There are three distinct buffers types: calmodulin and high and low affinity sites of troponin so

$$I_{BUFFER} = I_{CMDN} + I_{HTRPN} + I_{LTRPN}, \tag{5}$$

where

$$I_T = k_T^+ c([T]_{tot} - [Tb]) - k_T^-[Tb], \text{ for } T = \{\text{CMDN, HTRPN, LTRPN}\}. \tag{6}$$

Here $[T]_{tot}$ is the total concentration of buffer type T, and [Tb] is the corresponding concentration in bound form. The rate constants are $k_T{}^+$ and $k_T{}^-$. The values of the constants are given in Table 1.

The computational domain Ω consists of two distinct types, the bulk space, denoted Ω_{bulk}, and the fuzzy space, denoted Ω_{fuzzy}. A bar over the variable means an average and the subscript describes over which domain, e.g., $\bar{c}_F$is the average concentration of Ca^{2+} in the fuzzy space:

$$\bar{c}_F = \frac{1}{|\Omega_F|}\int_{\Omega_F} c(x)dx.$$

The appropriate values for the diffusion coefficients are not known and we have used a wide range of values to investigate the consequences for the mathematical model. It is clear that diffusion is slower in the cell than in water. E.g., Despa et al. (21) obtained a value for Na^+ diffusion in the cytoplasma to be two orders of magnitude lower than in water. Crowding in the cleft space might reduce this number further. For our purpose, it is the diffusion in cleft space that is critical, and in the simulation we have used values 10^2–10^4 lower than that in water. The results are quite insensitive to the diffusion level in the bulk space and we have simply used the values from Despa et al. (21) in this domain.

According to Langer and Peskoff (22), the Ca^{2+} diffusion is half that of Na^+. Thus, the default diffusion parameters in the bulk myoplasma was set to $k_c = 0.5{\cdot}10^{-7}$ cm^2/s and $k_s = 1{\cdot}10^{-7}$ cm^2/s, which is equivalent to $k_c = 5000$ nm^2/ms and $k_s = 10000$ nm^2/ms. This is ~1% of the diffusion in water (which for Na^+ is $1.2{\cdot}10^6$ nm^2/ms). The intracellular Na^+ and Ca^{2+} concentrations were assumed to be in equilibrium before the onset of the stimulus, i.e., the concentrations in the bulk space and the fuzzy space were equal. For Na^+, the initial condition was set to 12.0 mM and for Ca^{2+}, the initial condition was 0.1 μM. The rest of the initial conditions followed the model by Winslow et al. (16).

Current expressions and boundary conditions

For the boundary conditions we specified the ionic flux over the boundary, expressed as amount per time per area. The currents in the model of Winslow et al. (16) are expressed in current per capacitance so these need to be scaled. For notational convenience, we enumerate the different current types from $i = 1, \ldots, n$ and for the ith current we write

$$J_i = \frac{C}{Fa_i\sigma_i} I_i. \tag{7}$$

Here. I_i is the original current expression and J_i is the flux expression used in the boundary conditions. Furthermore, C is the specific membrane capacity, F is Faraday's constant, a_i is the area of a single channel opening, and σ_i is the density of the channel in the cell, defined as $\sigma_i = A/m_i$, where A is the area of the cell surface and m_i is the number of channels of type i in the cell. The specific area of the channel opening a_i is not critical as the current expression is integrated over the channel area, thus canceling the contribution. In the model, channel openings were set to have a 2 nm radius. The density constants used are given in Table 2. The boundary condition can be written as

$$k_s\frac{\partial s}{\partial n} = \begin{cases} 0, & x \in \Gamma_0 \\ J_1(t), & x \in \Gamma_1 \\ \vdots & \vdots \\ J_n(t), & x \in \Gamma_n\,. \end{cases} \tag{8}$$

Here, Γ_i are all the channel openings for current i. The set of Γ_i forms a partitioning of Γ, i.e., $\cup_{i=0}^{n}\Gamma_i = \Gamma$ and $\Gamma_i \cap \Gamma_j = \emptyset$ if $i \neq j$.

Let us now verify that the flux of ions over the boundary causes a change in the concentration, consistent with the original compartmental formulation. From mass conservation and Fick's law we have that

$$\frac{d}{dt}\int_\Omega s dV = \int_\Gamma k_s\frac{\partial s}{\partial n} dA, \tag{9}$$

where Ω is the volume of the compartment. Using Eq. 8, the surface integral is decomposed into the contributions from each channel type. Note that the contribution from Γ_0 vanishes as the current there is zero:

$$\int_\Gamma k_s\frac{\partial s}{\partial n} dA = \sum_{i=1}^{n}\int_{\Gamma_i} J_i dA = \sum_{i=1}^{n} J_i \int_{\Gamma_i} dA = \sum_{i=1}^{n} J_i A_i. \tag{10}$$

Here we have defined A_i to be the area of Γ_i. Observe that $A_i = m_i{\cdot}a_i$. Using Eq. 7, we have that

$$\frac{d}{dt}\int_\Omega s dV = \sum_{i=1}^{n} I_i\frac{C}{Fa_i\sigma_i} m_i a_i = \sum_{i=1}^{n} I_i\frac{C}{Fm_i/A} m_i = \frac{CA}{F}\sum_{i=1}^{n} I_i \tag{11}$$

and we see that the average concentration change for s will be the same as in the compartmental formulation, i.e.,

$$\frac{d}{dt}\bar{s} = \frac{d}{dt}\frac{1}{V}\int_\Omega s dV = \frac{CA}{FV}\sum_{i=1}^{n} I_i. \tag{12}$$

TABLE 1 Buffer constants used in the model were taken from Winslow et al. (16), except the rate constants for calmodulin, which were taken from Smith et al. (73)

Parameter	Definition	Value
$[CMDN]_{tot}$	Calmodulin concentration	50 μM
k^-_{CMDN}	Ca^{2+} off rate for calmodulin	38×10^{-3}/ms
k^+_{CMDN}	Ca^{2+} on rate for calmodulin	100/(mM ms)
$[LTRPN]_{tot}$	Troponin low affinity site concentration	70 μM
k^-_{LTRPN}	Ca^{2+} off rate for troponin low affinity sites	0.04/ms
k^+_{LTRPN}	Ca^{2+} on rate for troponin low affinity sites	40/(mM ms)
$[HTRPN]_{tot}$	Troponin high affinity site concentration	140 μM
k^-_{HTRPN}	Ca^{2+} off rate for troponin high affinity sites	66×10^{-6}/ms
k^+_{HTRPN}	Ca^{2+} on rate for troponin high affinity sites	20/(mM ms)

Numerical methods

The model consists of three main parts, corresponding to Eqs. 2–4. We solved these equations using operator splitting, solving one subproblem at

TABLE 2 Channel densities used in the model

Parameter	Channel type	Density	Source
σ_{Ca}	L-type	6/μm^2	(41)
σ_{Na}	Fast Na^+	7.5/μm^2	(40)
σ_{NCX}	Na^+/Ca^{2+} exchanger	400/μm^2	(38)
σ_{NAK}	Na^+/K^+ pump	750/μm^2	(39)

the time. The required temporal resolution varies throughout an action potential and we found it best to use adaptive time stepping. An outline of the algorithm is shown below:

$$
\begin{aligned}
&t = 0,\ \Delta t = \Delta t_0,\\
&\text{while } (t \le T)\\
&\quad w = \mathrm{ODE}(t, t+\Delta t,\ w^{\mathrm{n}}, c^{\mathrm{n}}, s^{\mathrm{n}})\\
&\quad c = \mathrm{CALCIUM}(t, t+\Delta t, w, c^{\mathrm{n}}, s^{\mathrm{n}})\\
&\quad s = \mathrm{SODIUM}(t, t+\Delta t, s^{\mathrm{n}}, w, c)\\
&\quad \text{if } \langle \text{all solvers converged} \rangle\\
&\qquad t = t + \Delta t\\
&\qquad w^{\mathrm{n}+1} = w;\ c^{\mathrm{n}+1} = c;\ s^{\mathrm{n}+1} = s;\\
&\qquad \Delta t = 1.1 \times \Delta t;\ //\ \text{increase time step.}\\
&\quad \text{else}\\
&\qquad \Delta t = 0.5 \times \Delta t;\ //\text{retry with a smaller time step.}
\end{aligned}
$$

The names in capital letters refer to procedures that solve the subproblems. For the ODE problem, we use an explicit fourth order Runge-Kutta method with internal adaptive time stepping. The two procedures CALCIUM and SODIUM are implicit partial differential equation (PDE) solvers. Both of these problems are nonlinear due to the boundary condition, i.e., the influx over the boundary depends nonlinearly on the concentration. For the CALCIUM problem, there is additional nonlinearity due to the buffering. We only describe the CALCIUM algorithm, as SODIUM might be seen as a special case of CALCIUM.

Equation 2 has the structure

$$\frac{dc}{dt} = \nabla \cdot k_{\mathrm{c}} \nabla c - g(c, w). \tag{13}$$

To ensure numerical stability we use a implicit scheme to discretize this equation in time:

$$\frac{c^{\mathrm{n}+1} - c^{\mathrm{n}}}{\Delta t} = \nabla \cdot k_{\mathrm{c}} \nabla c^{\mathrm{n}+1} - g(c^{\mathrm{n}+1}, w^{\mathrm{n}+1}). \tag{14}$$

This is a nonlinear problem in $c^{\mathrm{n}+1}$. There are several approaches to solving these kinds of equations. We have chosen to use successive substitution due to its simplicity and robustness. Another possible choice is Newton's method. It is typically faster but requires expressions for the derivatives, which in our case will be quite complex. Also the convergence depends upon a good initial guess for the solution.

Using subscript "l" to represent the iteration counter, the iteration is

$$c_{l+1} = \Delta t k_{\mathrm{c}} \nabla c_{l+1} - \Delta t g(c_l, w) + c^{\mathrm{n}}. \tag{15}$$

Thus for each iteration, we solved Eq. 15, which is a linear problem in c_{l+1}. The finite element method is used. First a weak form of Eq. 15 is derived and the subsequent problem has been implemented using Diffpack (23).

Geometrical description

The geometrical model is meant to capture a typical functional unit; one T-tubule surrounded by SR. We start this section by citing some relevant literature regarding the fuzzy space geometry before we state the details of the geometrical model that we use.

The T-tubules are found nearly every 1.8 μm along the Z-line and enter the heart cell perpendicular to the surface membrane. The T-tubule invaginations contain extracellular fluid (24). The data on T-tubule dimensions are highly dependent on the species and also vary considerably within a single species. Most studies have been conducted with conventional transmission or scanning electron microscopy. In the guinea pig, diameters in the range of 200–360 nm (25) and 170–850 nm (26) have been found. Rat ventricular myocytes have been the subject of several studies, with T-tubule diameters ranging from 70 to 114 nm (27–29) . Soeller and Cannell (30) point out that methodological problems with conventional electron microscopy may cause erroneous estimates. In our study, we have used their T-tubule diameter estimate of 255 nm, which was obtained using two-photon laser scan microscopy on living rat myocytes.

The T-tubule may be flattened or rounded in the junctional regions, e.g., see Nakamura et al. (27) and Forbes and Sperelakis (31). Junctional sarcoplasmic reticulum usually forms extensive flat cisternae. Zhang et al. reported an average height of the cisternae of 18.6 nm in mice myocardium (32).

Quantitative data on the size of the junctional patches are scarce. Assuming a circular structure, Franzini-Armstrong et al. (29) estimated the size of a junction to be 75,690, 224,547, and 107,648 nm^2 in dog, rat, and mouse myocardium, respectively. In chick myocardium, peripheral couplings have been found to be 16,600–17,700 nm^2 (33).

Zhang et al. (32) have reported an average length of 334 nm of junctions in the mouse ventricle. Assuming a circular morphology, this would correspond to a patch size of 87,571 nm^2, which is in reasonable accordance with the older data of Franzini-Armstrong et al.

In our model, SR was modeled as a cap with 18.6 nm thickness and a mean diameter of 334 nm. The cap is not flat but curves around the T-tubule. The thickness of the fuzzy space was set to 15.5 nm (34), i.e., the distance from the T-tubule to SR. The RyR, which consists of four identical monomers, is 29 × 29 × 12 nm and protrudes into the gap between the junctional sarcoplasmic reticulum and the T-tubule (35). The receptors were organized with a center to center distance of 31.5 nm (36).

Despa et al. (37) found that 63% of the NCX and 59% of the Na^+/K^+-pump (NKA) resides in the T-tubule with a corresponding T-tubule/sarcolemmal density of 3.6 and 3.1, respectively. By using a sarcolemmal NCX density of 400/μm^2 (38), NKA density of 750/μm^2 (39), Na^+ channel density of 7.5/μm^2 (40), and LTCC density of 6/μm^2 (41), we calculated the channel spacing to be 29.5 nm and 16.5 nm for NCX and NKA. The density of the fast Na^+ channel is thought to be uniformly distributed throughout the whole cardiomyocyte (42), which gives the possibility that one or no Na^+ channel resides in the dyad.

By assuming symmetry around the T-tubule, the three-dimensional problem could be reduced to a two-dimensional computation. Fig. 1 shows a schematic of the geometry. A channel opening in the symmetry plane represents a band of channels at that radial distance from the axis of symmetry. Channel placement is made such that the distance between these bands

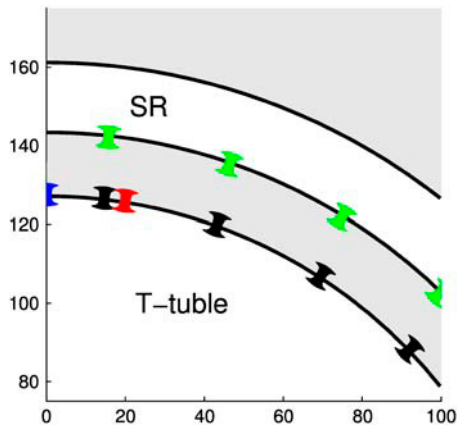

FIGURE 1 Schematic picture of channel placement in the fuzzy space. The blue channel represents the LTCC, the black and green channels represent NCX and RyR, respectively. The red channel represents the Na^+ channel (see text for details).

corresponds to the typical interchannel distances stated above. For example, when the RyRs are spaced with 31.5 nm on the SR surface, they are represented by six sites in the model. It is convenient to refer to these sites by the angle they make in radial coordinates; these are 33.2, 45.8, 58.4, 71.1, and 83.7° (Fig. 1). The NCXs and the NKAs are distributed in a similar fashion on the T-tubule surface, with the spacing 29.5 nm and 16.6 nm, respectively. This gives a total of six NCX sites and nine NKA sites. One LTCC is placed at 90°, i.e., at the axis of symmetry.

The LTCC, RyRs, NCXs, and NKAs were fixed with the above geometry. The Na^+ channel, however, was subjected to three scenarios: 1), no Na^+ channel in the dyad (due to the small volume in the fuzzy space, we will not exclude this possibility), 2), one Na^+ channel midway between two NCXs and, 3), one Na^+ channel adjacent to an NCX.

The bulk space surrounding the T-tubule, SR, and fuzzy space was set to 4000 nm × 4000 nm. Na^+ and Ca^{2+} ions were allowed to diffuse across the artificial cytosolic boundaries.

RESULTS

Experiments in isolated cardiomyocytes

According to our hypothesis, the existence of a fuzzy space should promote reverse-mode NCX and SR Ca^{2+} release, which precedes Ca^{2+} release triggered by Ca^{2+} influx through the LTCCs. To test this hypothesis, we experimentally altered NCX activity in isolated cardiomyocytes while measuring the latency of Ca^{2+} release. We defined latency as the time delay between the onset of the stimulus and the onset of the $[Ca^{2+}]_i$ transient. To block the reverse mode of NCX, 5 μM KBR was used. (43). Fig. 2 shows representative line-scan images during 1 Hz stimulation before (panel *A*) and after (panel *B*) KBR treatment. The line-scan images shown at right are enlargements from the indicated regions of the line scans at left. Exposure to KBR increased the latency of Ca^{2+} release in field-stimulated myocytes and also in patch-clamped myocytes stimulated with either action potentials or depolarizing voltage-clamp steps. Whereas Ca^{2+} release was initiated rapidly after the stimulus in control conditions, fluorescence levels departed somewhat later from baseline levels after KBR treatment. In voltage-clamped myocytes, KBR effects were maximal after 4 min of exposure when mean latency values were increased by 3.2 ± 0.4 ms ($P < 0.05$, $n = 6$) from control values (Fig. 2 *C*). A similar time course of KBR inhibition of NCX has been previously reported (43).

In other experiments, we attempted to indirectly inhibit reverse NCX using low-dose TTX. Maier et al. (44) have reported that the highly TTX-sensitive brain-type Na^+ channels are preferentially localized in the T-tubules in cardiomyocytes and can be blocked by a low-dose (200 nM) of TTX, which does not affect cardiac-type Na^+ channels. Thus, locally inhibiting Na^+ influx in the T-tubules should prolong latency of Ca^{2+} release. We observed that treatment with 200 nM TTX prolonged the latency of Ca^{2+} transients triggered by action potentials. Maximal effects were reached after 30 s of TTX application when mean latency values were increased by 1.1 ± 0.2 ms ($P < 0.05$, $n = 4$) from control values (Fig. 2 *C*). However, in cells pretreated with KBR,

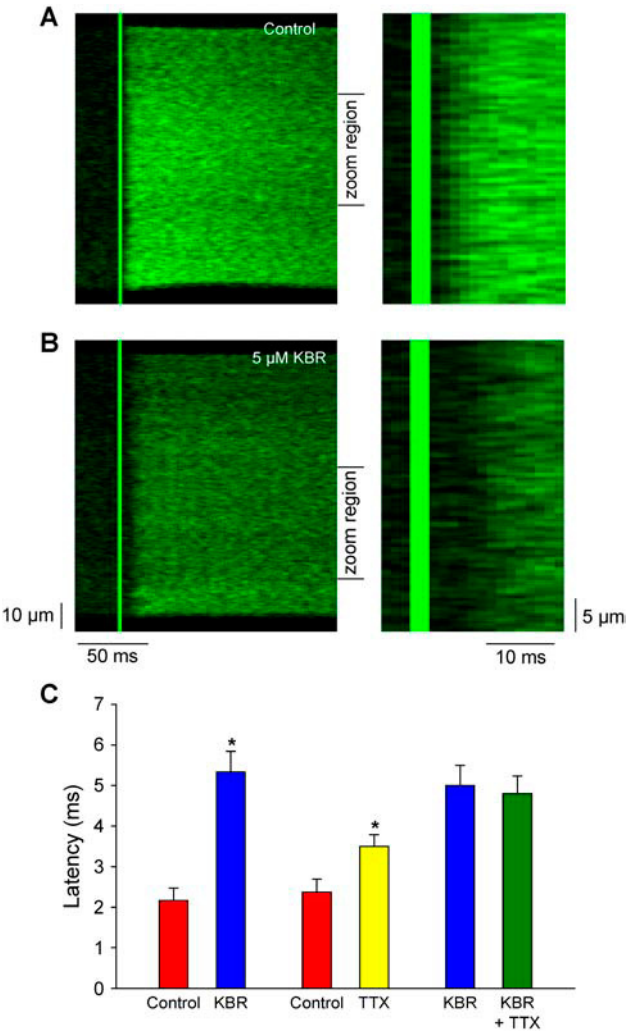

FIGURE 2 Line scan images taken before (*A*) and during (*B*) KBR application show that NCX inhibition increases SR Ca^{2+} release latency. Mean changes in latency during treatment with 5 μM KBR, 200 nM TTX, and KBR + TTX are shown in *C*.

treatment with TTX did not alter latency values, suggesting these drugs increase latency by the same mechanism. As well, alterations in latency did not result from altered *dV/dt* max values for the upstroke of the action potential (control = 241 ± 47 V/s, $n = 8$; TTX = 234 ± 78 V/s, $n = 3$, P = NS; KBR = 204 ± 37 V/s, $n = 6$, P = NS; KBR + TTX = 211 ± 40 V/s, $n = 6$, P = NS). Other experiments were conducted with voltage-clamp steps in which the NCX would be expected to be directly activated by membrane depolarization. In these experiments, treatment with 200 nM TTX did not alter latency of Ca^{2+} release during 4 min of application (control = 2.4 ± 0.4 ms, 4 min = 2.7 ± 0.4 ms, P = NS, $n = 4$). This indicates that the NCX is likely involved in the TTX effects observed during stimulation with action potentials. Blockade of the L-type Ca^{2+} channel with 5 μM nifedipine did not alter latency in field-stimulated cells (control = 2.4 ± 0.2 ms, nifedipine = 3.2 ± 0.3, $n = 5$, P = NS).

Mathematical results

Fig. 3 shows the time development for some key variables of the model. The figure shows ''whole cell'' currents, which in the subsequent simulations were scaled down to single channel currents. The tracings are based on the model of Winslow et al. (16), but I_{to} was scaled up by a factor of three to obtain rat action potential (AP), which peaks at 1 ms after onset of the stimulation. These variables constituted the basic currents used in the diffusion model of the fuzzy space.

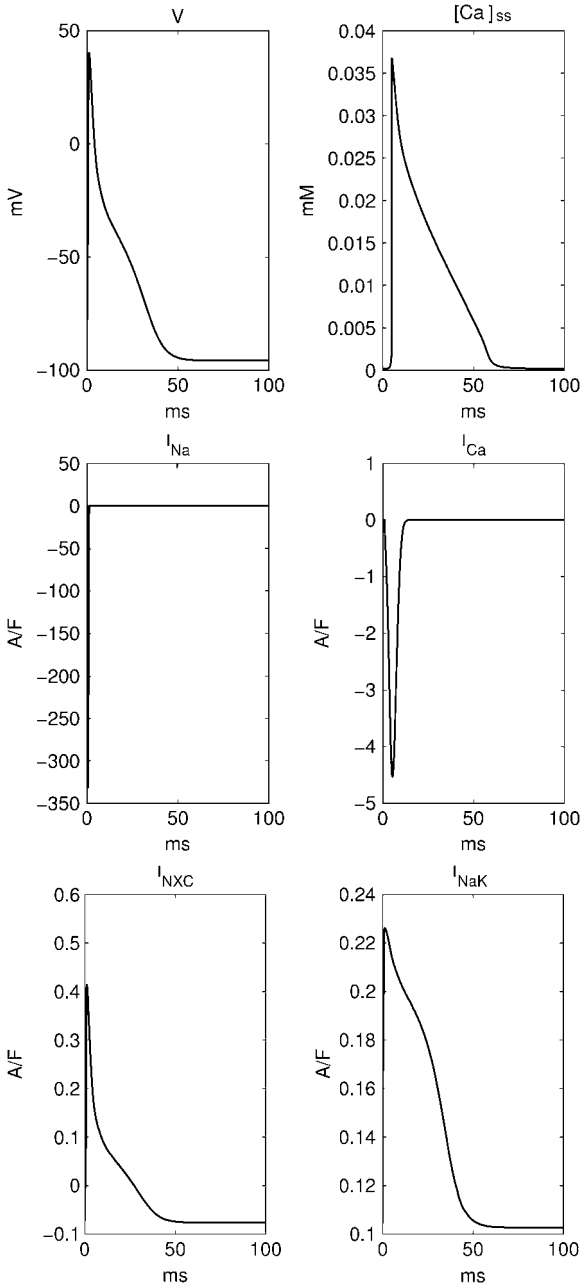

FIGURE 3 Traces from the underlying set of ODEs generated from a modified model by Winslow et al. (16) (see text for explanation). Membrane potential (*upper left panel*), $[Ca^{2+}]_{ss}$ (*upper right panel*), I_{Na} (*middle left panel*), I_{Ca} (*middle right panel*), I_{NaCa} (*lower left panel*), and I_{NaK} (*lower right panel*).

In this section, we will present a set of simulations that will demonstrate under which circumstances the model predicts that NCX will contribute to CICR.

Fig. 4 shows the Ca^{2+} distribution in the fuzzy space 1.1 ms after the initial stimulus has been applied. By gradually increasing Ca^{2+} influx into fuzzy space using a formulation of the model in which the RyRs were activated, we obtained a threshold value for CICR to be 0.5 μM in the fuzzy space. This value was used throughout the whole set of simulations. In the figure, areas with deep red color have reached this level. We see that Ca^{2+} has entered through the L-type channel, creating a pool of high Ca^{2+} concentration on the intracellular side. Note that Ca^{2+} is also entering via the exchangers. Even though no Na^+ channel is present, the basal concentration of intracellular Na^+ concentration (12 mM) is sufficient to generate a small reverse current in the early phase of the action potential. In this simulation, the fuzzy space diffusion is assumed to be three orders of magnitude lower than in water. The concentration of Ca^{2+} at the SR side of the fuzzy space has not yet reached the threshold value necessary for CICR occur.

To demonstrate the temporal evolution of the concentration, we have in Fig. 5 plotted the time development of [Ca] at the five RyR sites in our model in the absence of any Na^+ channel and with $[Na^+]_i$ equal to 12 mM. In the figure, the RyR sites are referred to by the angle of their location with respect to the x axis in Fig. 1, e.g., 90° corresponds to the y axis where the L-type channel is located. The larger the angle the closer the RyR is to the L-type channel. The thin blue horizontal line represents threshold for CICR. We see that the RyR closest to LTCC, i.e., the one labeled 83.7° is triggered just after 1 ms, in accordance with Fig. 4. The other sites are triggered shortly thereafter. The concentrations at the other sites rise more slowly, indicating that Ca^{2+} also diffuses out into the bulk space instead of accumulating in the

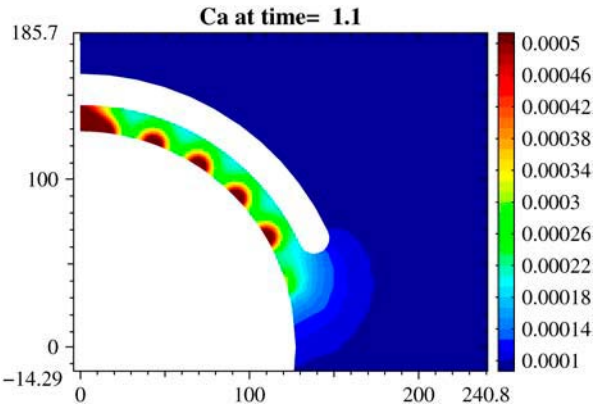

FIGURE 4 Snapshot of Ca^{2+} concentration in the fuzzy space with k_c = 500 nm^2/ms. Values are in millimolars, i.e., the color range is 0.1–0.5 μM. Note the elevated Ca^{2+} concentration in the fuzzy space around the NCXs.

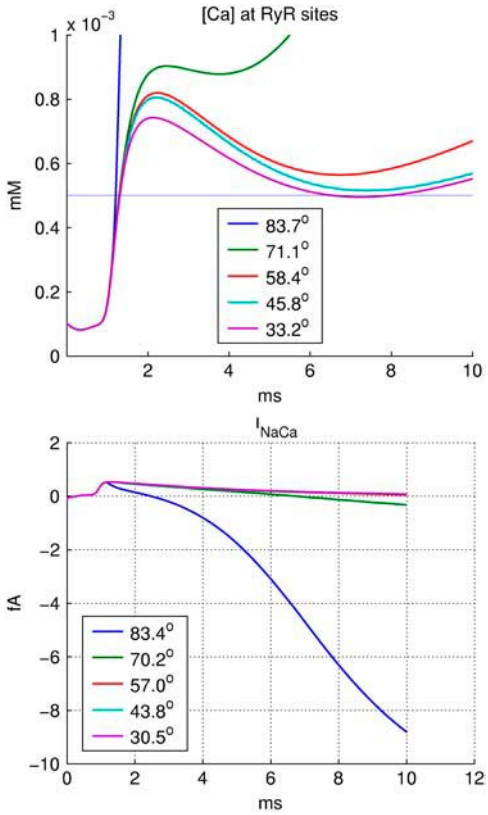

FIGURE 5 (*Upper panel*) Time course of Ca^{2+} at the different RyR locations with $k_c = 500 nm^2/ms$ and no Na^+ channel present in the dyad. The thin blue horizontal line is the activation threshold for the RyRs. (*Lower panel*) Time course for the NCX current during the same situation as above. We can clearly see how the NCX current through the exchanger neighboring the LTCC (*blue line*) shifts from reverse to forward mode early in the AP. (*Insets*) Upper panel, RyR sites; lower panel, NCX sites.

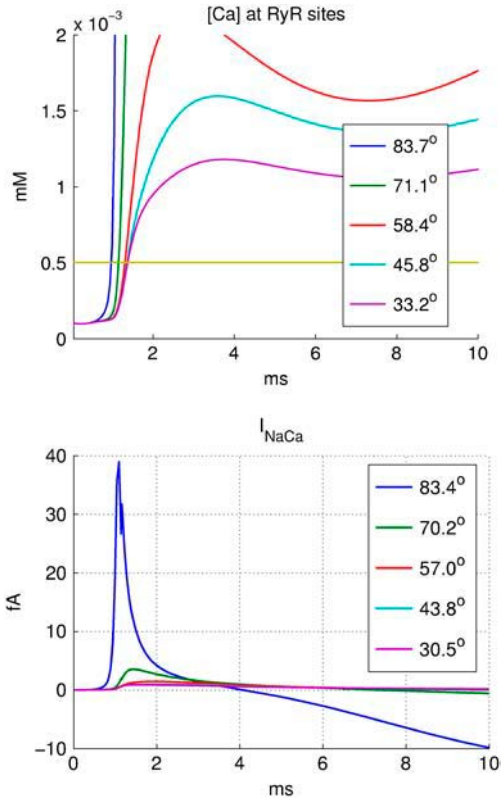

FIGURE 6 (*Upper panel*) As in Fig. 5, but with a Na^+ channel present in the dyad. In the lower panel, we can clearly observe the effect of including a Na^+ channel in the dyad. The NCX current peaks very rapidly in reverse mode before it return to its normal (forward) mode. Note that as in Fig. 5, the NCX activation occurs in a very narrow ''time window'' and the shift from reverse to forward mode is accomplished within 2 ms. The Na^+ channel is located as in Fig. 1, that is, adjacent to an NCX. Insets as in Fig. 5.

fuzzy space. Note that the actual Ca^{2+} release is not included in this simulation. If it were, then the release from the first receptor would cause a sufficient increase in the fuzzy space concentration to also trigger the rest of the sites. As mentioned in the Materials and Methods section, we are studying the role of the NCX in CICR, not CICR in itself. The basic result from Fig. 5 is that the conditions were sufficient for CICR to occur at 1 ms. In the lower panel of Fig. 5, the exchanger currents at the corresponding sites are plotted. There is only a very small transient phase of reverse mode NCX current before the exchanger sitting close to the LTCC switches into strong forward mode.

We will now turn to the two scenarios where a Na^+ channel is adjacent to an NCX unit and when it is located midway between two NCX units. Fig. 6 shows the case with a Na^+ channel located adjacent to the NCX unit closest to the LTCC, as in Fig. 1. Comparing Fig. 6 with Fig. 5, we see that the Ca^{2+} concentration rises more rapidly and to a higher level when the Na^+ channel is present, the reason being that the elevated Na^+ concentration greatly enhances the reverse mode of the exchanger located closest to the Na^+ channel. This can be seen by comparing the lower panels of Fig. 5 and Fig. 6. However, the difference in timing is quite small; the CICR level is reached 0.3 ms earlier with the Na^+ channel in place. With the channel placed further away from the NCX channel the difference was even less. Plots from this latter simulation are not shown. In the simulation above, the maximum $[Na^+]$ seen by the NCX was 74 mM.

The diffusion constant in the bulk space of the cytosol is fixed in all the simulations in this article. The assumption that the diffusion constant in fuzzy space was three orders of magnitude lower than in water was used in the simulations presented above. If we instead assume equal diffusion in the two compartments, the results with respect to CICR triggering are virtually unchanged, except that the more distal RyR sites are triggered earlier.

The appropriate value for the diffusion constant in fuzzy space is uncertain, but if it is larger than 1000 nm^2/ms, our simulations suggest that the NCX does not play an important role in CICR. Below we shall see that provided the diffusion value in fuzzy space is lower, the NCX mechanism becomes important. With slow diffusion, the Ca^{2+} entering through the LTCC will use a longer time to reach the RyRs, thus

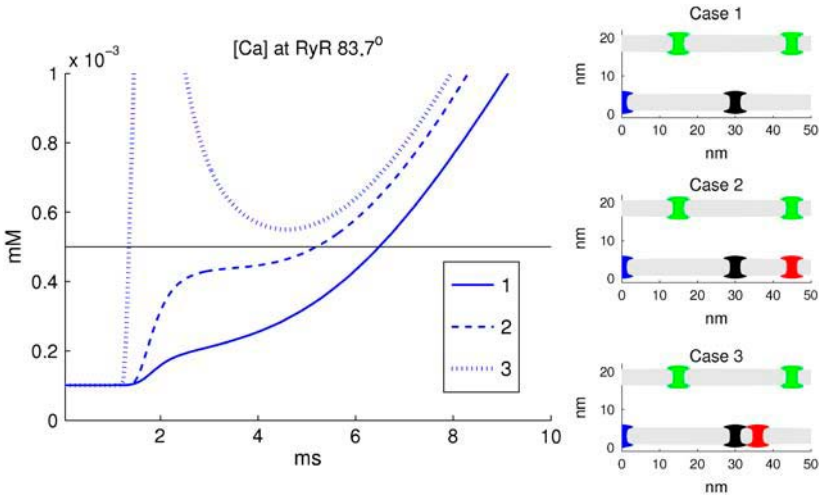

FIGURE 7 Calcium concentration at the RyR site closest to the LTCC using $k_c = 50\text{nm}^2/\text{ms}$ The right-hand panel shows the channel placement for the three different cases. The blue channel at the y axis represents the LTCC, the black channel at 30 nm is the NCX, and the red channel represents the Na^+ channel. The two green channels above represent RyR sites.

causing a delay in CICR through this mechanism. On the other hand, with reduced diffusion, more Na^+ will build up around the Na^+ channel and enhance the reverse mode of neighboring NCX units. Thus, we lowered the diffusion constants in the fuzzy space to four orders of magnitude lower than in water (corresponding to $k_c = 50\ \text{nm}^2/\text{ms}$ and $k_s = 100\ \text{nm}^2/\text{ms}$). The quantitative effect of this is seen clearly in Fig. 7. In this case, the maximum $[Na^+]$ seen by the NCX was 177 mM. Triggering through LTCC alone (*Case 1* in Fig. 7) occurs at 6.5 ms, whereas it occurs at 1.4 ms in the case where the Na^+ channel lies adjacent to the NCX unit (*Case 3*). When the Na^+ channel lies farther from the NCX unit (*Case 2*), the exchanger current is weaker and the triggering occurs at 5.2 ms. Depending on the channel location, we thus get a time lag of up to 5 ms in the absence of a Na^+ channel. In Fig. 8, NCX currents for the three cases are drawn. In Case 3, a strong, but short lasting reverse mode is present. This should be compared to the blue trace in the lower panel of Fig. 6, which shows the current under the same conditions but with 10 times the rate of diffusion. In the low diffusion case (Fig. 8), the reverse mode is strong due to larger accumulation of Na^+, and the forward mode is reduced, due to a longer lasting Na^+ transient. In Fig. 9 we have repeated the experiment, but with the LTCC blocked. The only Ca^{2+} source is the NCX. With no fast Na^+ channel present (*Case 1*), there is not sufficient driving force for the exchanger. With the Na^+ channel lying adjacent to the NCX unit (*Case 3*), the latency is quite similar to the situation with an open LTCC. When the Na^+ channel lies farther from the NCX unit (*Case 2*), the exchanger current is too weak on its own to trigger release. Simulations with the reverse mode of the NCX blocked have also been performed (not shown). The effect is very similar to not having a Na^+ channel present. In all cases, the rise in $[Na^+]_i$ was only transient, with no buildup from beat to beat.

DISCUSSION

In principle, our model predicts that NCX can contribute to early Ca^{2+} release from RyR in rat cardiomyocytes. However, after a few milliseconds, the reverse mode is rapidly turned off and the NCX switches into equilibrium or

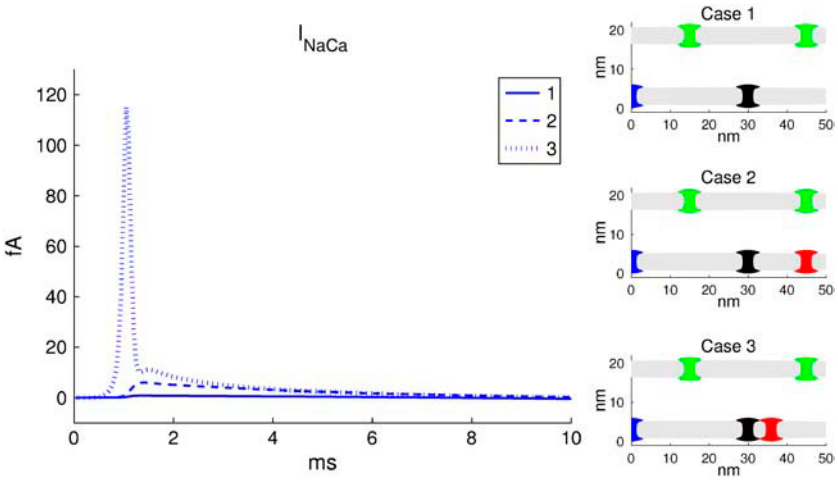

FIGURE 8 Exchanger current at the RyR site closest to the LTCC. The right-hand panel is repeated from Fig. 7.

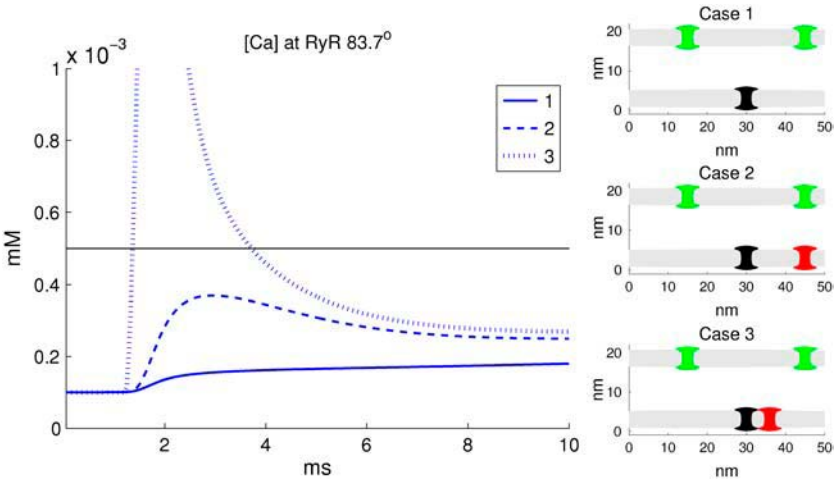

FIGURE 9 LTCC blocked. The exchanger current is very similar to the tracings in Fig. 8 and thus not repeated. The symbols are as described in Fig. 7.

forward mode. The forward mode will be amplified by the subsequent Ca^{2+} release. However, Ca^{2+} release was not included in our model. We focused on the very early trigger Ca^{2+} that enters the cell through LTCCs and NCX. The model corroborates the experimental finding that inhibition of reverse mode exchange by KBR delays the onset of the Ca^{2+} transient by 3–4 ms. The conditions for this contribution of NCX to early Ca^{2+} release are twofold. First, a Na^+ channel must be present in the dyad very close to the NCX protein, and second, diffusion in the dyadic cleft (fuzzy space) must be several orders of magnitude slower than in water, and slower even than in the bulk cytoplasm. Thus, CICR seems to depend on a multi-molecular complex involving membrane proteins of both the SR and T-tubular membranes between which ionic gradients can transiently exist due to slow diffusion. The model also predicts that NCX alone in the absence of I_{Ca} can trigger Ca^{2+} transients as shown by several investigators (12,8,13,7).

Inhibition of reverse mode Na^+/Ca^{2+} exchange delays onset of Ca^{2+} transient

The differential effect on Ca^{2+} release latency observed with the two drugs KBR (5 μM) and TTX (200 nM) likely reflects differing degrees of NCX inhibition. The dose of KBR that was used has been previously shown to inhibit reverse-mode NCX activity by 90% (43), suggesting that nearly all Ca^{2+} entry by NCX was blocked in our KBR experiments. Thus, it seems likely that in the in vivo setting, CICR triggered by NCX may precede the triggering by LTCCs by ~3–3.5 ms. The shorter prolongation of Ca^{2+} release latency observed in the TTX experiments could result from less effective inhibition of NCX. Maier et al. (44) observed that 200 nM TTX blocks 91% of neuronal Na^+ channels; the subtype of channels they report to be predominantly localized in the T-tubules. This was recently substantiated by Brette and Orchard (45), who found that 14% of the Na^+ channels of the rat cardiomyocyte are TTX-sensitive neuronal channels and that 80% of these are located in the T-tubules. However, although it was observed that cardiac type Na^+ channels are predominantly localized in the intercalated discs, ~3% are also present in the T-tubules and contribute by almost 70% of the T-tubular Na^+ current. These channels are not inhibited at low TTX doses. Thus, Na^+ entry may have maintained significant levels of reverse mode Na^+/Ca^{2+} exchange activity within the dyad in our experiments during application of a low dose TTX. Unfortunately, it is not possible to fully block Na^+ channels in these experiments since higher doses of TTX would prevent action potentials. We did not observe any significant reduction in the dV/dt of the upstroke of the action potential during application of a low-dose TTX. However, a 10% reduction as observed by Brette and Orchard (45) would be beyond our detection limit since we only included a limited number of cells to ensure that the upstroke velocity was not greatly reduced. Also, since there are no markers for the stimulus in their figures, it is not possible to deduce the effect of TTX on the lag. Similar experiments conducted with voltage-clamp steps likely activated reverse-mode NCX directly, possibly overriding Na^+ influx, thus preventing effects of Na^+ blockade on latency. Thus, the experiments show that reverse mode Na^+/Ca^{2+} exchange will trigger Ca^{2+} release 3–4 ms earlier than that triggered by I_{Ca}. The blockade of reverse NCX by KBR is somewhat controversial, and consideration should be given to possible alteration in reversal potential and other side effects of KBR. However, in a study by Iwamoto and Kita (46), they found that KBR suppressed outward NCX current 60 times more strongly than the inward current. Hence, KBR has gained acceptance for inhibition of reverse mode NCX by several investigators, including those of Bers and Györke (43,47).

A new model allows for simulation of ion gradients within the fuzzy space

The results from the mathematical modeling basically support the experimental data and the model allows examination

of the consequences of altering both the placement of the channels and the diffusion constant in the fuzzy space.

The distribution of the various channels within the dyad is a matter of debate. Scriven et al. (48), using wide-field fluorescence microscopy and image deconvolution, found that even though the fast Na^+ channels and the NCXs were distributed largely within the T-tubules, they were unable to detect any colocalization to the RyRs. On the other hand, in a more recent study by Thomas et al. (4), using immunogold labeling and electron microscopy, they found that some NCX proteins were as close to the RyRs as the LTCCs and thus, could contribute to CICR. The results from Thomas et al. served as a basis for our geometric data to perform the PDE modeling within the dyad.

This study is one of a few that examine the diffusion in the fuzzy space in a three-dimensional model. The model includes sets of ODEs and PDEs to solve both the temporal and spatial distribution of the diffusing ions in the fuzzy space. Langer and Peskoff (22) pioneered this approach in their excellent article. However, we have used a different geometry and the underlying currents (I_{Ca}, I_{Na}, and I_{NCX}) were taken from the Winslow model providing more accurate formulations. Of particular note, Langer and Peskoff have used $I_{Ca} = 0.3$ pA (1 ms ramp) and $I_{Na} = 2$ pA (trapezoidal pulse), which is not in accordance with data showing that peak I_{Na} is ~50 times higher than peak I_{Ca} (see, e.g., Winslow et al. (16)). Furthermore, they focused on SR-Ca^{2+} release through the RyR complex, whereas our focus is on Ca^{2+} fluxes that trigger release. Also, we have tested effects of various channel and transporter localizations as well as various diffusion constants for Na^+ and Ca^{2+} in the fuzzy space. Indeed, as we can see in Fig. 7, the [Ca^{2+}] elicited from LTCC alone reached the threshold value of 0.5 μM within 6.5 ms, whereas in combination with reverse NCX, the same concentration was reached at 1.4 ms. The conditions for this contribution of the exchanger were a close association between NCX and a Na^+ channel in combination with slow diffusion.

The simulation predicts that diffusion may be very slow in the fuzzy space

There are several reports that indicate that diffusion in fuzzy space is quite slow, and estimates of the diffusion constant in the dyadic space have been extensively debated (1,2,49–51). Several of these studies are based on circumstantial evidence (50,51), and there are only a few investigators that have addressed the question directly. Wendt-Gallitelli et al. (52) and Silverman et al. (53) have both shown that Na^+ can accumulate close to the sarcolemma. Despa et al. (21) recently demonstrated slow Na^+ diffusion in the bulk of the cytosol indicating that regional differences with respect to diffusion may also exist within the cell in accordance with previous data (37). The diffusion constant from Despa et al. (21) is in contrast to the much higher value obtained in the very early work by Kushmerick and Podolsky (54), who found that sodium diffusion in frog skeletal muscle was 50% of that in water. However, Despa et al. used a different and novel technique to estimate sodium diffusion in rat ventricular myocytes and it may at present represent the best estimate for intracellular sodium diffusion in rat cardiomyocytes. Several models have assumed that diffusion is slower in the subsarcolemmal compartment, but few models have tested whether slow diffusion is a prerequisite for the model to fit observations.

Shannon et al. (55) developed a detailed mathematical model for Ca^{2+} handling and ionic currents in the rabbit ventricular myocyte, but only modeled diffusion between different compartments, not in the restricted fuzzy space. They used a diffusion constant for Na^+ from the dyadic cleft to the submembrane compartment (defined as a space beneath the sarcolemma through the whole cell) very close to Na^+ diffusion in water. Thus, their diffusion constant between these compartments were two orders of magnitude higher than the bulk diffusion from the study of Despa et al. (37). On the other hand, it might not be correct to compare these constants since they are from partially different compartments. Our focus, however, was diffusion in the fuzzy space alone, i.e., one three-dimensional compartment, which included solving nonlinear PDEs. The model predicts that diffusion constants for Na^+ and Ca^{2+} must be considerably slower than previously thought, in accordance with the experimental data and in support of the ''fuzzy space'' hypothesis of Lederer et al. (1).

Our model showed that with the presence of the fast Na^+ channel in the dyad, the diffusion constant in fuzzy space had to be four orders of magnitude slower than in water, i.e., 100 nm^2/ms for Na^+ and 50 nm^2/ms for Ca^{2+} to reproduce the experimental data. With higher diffusion rates, not enough Na^+ would accumulate locally to allow for reversal of the exchanger. A word of caution is required for the estimate of the diffusion constant for Ca^{2+}. A large fraction of cytosolic Ca^{2+} and probably also in the dyadic cleft is bound to buffers. As has been reported for protons, buffers will slow the apparent diffusion constant (56). We have no direct data to substantiate that the diffusion of Ca^{2+} is 50% of that for Na^+. It may be even slower. Our result strongly indicates the presence of a fuzzy space with restricted diffusion in cardiac ventricular cells.

There may be multiple reasons for the slow diffusion in the fuzzy space. The dyadic cleft seems to be filled with proteins that are part of the signaling cascades or serve to stabilize the adjacent channel proteins both in the T-tubule and in the SR membranes. Hence it is quite likely that macromolecular crowding as described by Ellis (57) in a recent review contributes significantly to slowing diffusion. Hence, tortuous ''electrolyte pathways'' will be present (58). Also, the protrusion of the RyR contributes to the macromolecular crowding, and unless the Ca^{2+} binding sites are exactly opposite to the LTCC, there will be a longer distance for the ions to move. Also, there is little knowledge of the structure of the water molecules between the proteins. Various degrees of crystallization can importantly influence the diffusion of solutes.

Formulation of the channel properties in the model

Several formulations for the LTCC have been proposed (Luo and Rudy (59), Barrere-Lemaire et al. (60), and Bondarenko et al. (61)). Both the LTCCs and RyRs operate in a stochastic manner (62,19). Since we used the whole cell model of Winslow et al. (16), we also used the original current expressions, especially the formulation for the LTCC, which is a Markov model that accurately describes channel opening. In our simulations, channel inactivation is not important. The difference in I_{Ca} in different models is minimal when we only examine the first 10 ms of the current. Stochastic behavior of the RyRs was not an issue in this article since we were studying the process leading up to CICR, but not CICR itself. Hence, Ca^{2+} release from SR was not included.

We chose to simulate a dyad with only one LTCC. It is possible that there are more LTCCs within a single dyad, and Bondarenko et al. (61) in their model have recently simulated graded Ca^{2+} release from the SR by including a variable number of LTCCs in the dyads. They point out that there may be a large heterogeneity between dyads, and that this may explain graded release. It is quite possible that there is dyad heterogeneity also with regard to both presence and location of NCX as well as of Na^+-channels. Hence our model may have restricted applicability to a small subpopulation of dyads, although the experiments with inhibition of reverse mode NCX point to early trigger of Ca^{2+} release as a general phenomenon achieved by the NCX.

Another important factor is the formulation of the NCX kinetics. Luo and Rudy (59) presented a model for the NCX, which was also adapted by Winslow et al. (16). Other formulations of the NCX have also been proposed. Weber et al. (63) included allosteric regulation of the NCX. Again, we used the original current expressions from Winslow et al. (16) but modified it to include an allosteric component for activation by Ca^{2+} with $k_{05} = 152$ nM.

Local elevation of Na^+ is a prerequisite for reversal of the NCX

Our model predicts that local Na^+ concentration at the intracellular NCX site is important. The results indicate that I_{Na} must be present in the dyad very close to the NCX to obtain maximal effect of reverse mode NCX. Indeed, in a previous study by Sipido et al. (64), they were unable to detect any contribution from reverse NCX in CICR at potentials below +60 mV. This was mainly due to the fact that the experimental protocol did not allow for opening of the fast Na^+ channel, which could provide the NCX with enough driving force in form of increased $[Na^+]_i$. Thus, the NCX relies on a powerful Na^+ gradient to build up around the exchanger for maximal activation. So far little is known about subcellular localization of Na^+ channels. The dyadic cleft is so narrow that optical resolution restricts the possibility to detect single channels and their colocalization with other channels. Electron microscopy using immunogold technique allows for better resolution, but is difficult to use because sample preparation often destroys the epitopes used for making the antibodies. So far no investigators have examined the exact localization of cardiac or neuronal type Na^+ channels in the cardiac cells. Our prediction is that a small subpopulation of either type of channel may be present in some or all of the dyads. The importance of Na^+ in triggering of SR-Ca^{2+} release has previously been demonstrated by Lipp et al. (65) and Kohomoto et al. (66). Their results support our hypothesis that Na^+ and thus NCX is of vital importance for contribution of Ca^{2+} release from SR. In addition, Haworth et al. (67) showed apparent activation of NCX current at physiological $[Ca^{2+}]_i$, which suggests that entry of physiologically relevant amounts of Ca^{2+} through the LTCCs can activate the NCX. Previous studies have also pointed out a synergistic interaction of the reverse NCX and the LTCC, which results in a larger total Ca^{2+} entry than the sum of entries mediated by each of these transport systems individually (68,47).

Interestingly, the effect of including the Na^+/K^+ pump in the model was surprisingly minimal since a very high number of pump molecules close to the NCX would be required to dampen the local rise of Na^+. In a study by Silverman et al. (53), no transient activation of Na^+/K^+ pump current was observed during the first 10 ms after the onset of I_{Na} in isolated ventricular myocytes from guinea pigs. However, the Na^+/K^+ pump will be very important in setting the average Na^+ concentration, and elevation of diastolic $[Na^+]$ will amplify the contribution of the NCX to trigger Ca^{2+} release. It may be of interest that James et al. (69) suggested that the two isoforms of the Na^+/K^+ pump may be spatially and functionally separate. They further claim that the $\alpha 1$ isoform, which is the dominant isoform in cardiac cells, has no influence on excitation-contraction coupling and NCX. Hence, it may be important in future models to study more closely various placement of the two isoforms in cardiac cells.

Early trigger Ca^{2+} through the NCX

The physiological implications of early trigger of Ca^{2+} release by reverse mode Na^+/Ca^{2+} exchange are not entirely clear. A few milliseconds may not seem critical for the contraction. However, for instance, at high heart rates, a rapid activation of contraction may become increasingly important, and reverse mode NCX may become more prominent due to rate dependent accumulation of intracellular Na^+. Since the Ca^{2+} transient consists of independent Ca^{2+} sparks, the contribution of the NCX may be viewed in light of the ~20 ms duration of a spark. Clearly, correct trigger timing will ensure early spark activation and rapid contraction. Also, in pathological conditions like heart failure, the significance of the NCX may become more prominent. It is well known that SERCA2 has a decreased pumping capacity in congestive heart failure (70) and that

Na^+/Ca^{2+} exchange activity is increased, probably to compensate for the decreased SERCA2 function (71,72). Thus, in heart failure, NCX may sustain contractility both by ensuring rapid release of Ca^{2+} from the SR and by providing more Ca^{2+} to the Ca^{2+} transient. Thus, the NCX has multiple roles in cardiac excitation-contraction coupling: influx of Ca^{2+} in reverse mode to trigger Ca^{2+} release and to contribute to the Ca^{2+} transient and efflux of Ca^{2+} in forward mode. It is also well known that Ca^{2+} in the dyadic cleft contributes to rapid inactivation of LTCC. This is mainly due to released Ca^{2+}, but timing of release may clearly have effects on LTCC inactivation. Future expansion of our model will therefore have to include both Ca^{2+} release and LTCC inactivation properties to fully comprehend the consequences of early reversal of the NCX.

CONCLUSION

The experimental data showed that with a blockade of the reverse NCX by KBR the latency for SR Ca^{2+} release was increased by 3–4 ms compared to the control situation. Also, a partial inhibition of the fast Na^+ channel by TTX revealed an increased latency of >1 ms compared to control, which also supports that inhibition of reverse mode NCX leads to a more pronounced lag between depolarization and Ca^{2+} release. The mathematical model constitutes an SR unit wrapped around a T-tubule. The mathematical formulation was a nonlinear version of the diffusion equation derived from Fick's law. We modified the currents from the model of Winslow et al. (16) to obtain a rat AP, thus avoiding the prominent spike and dome AP typically present in larger mammals. The model is very robust and tolerates any changes in time step, channel placement, and diffusion constants. Due to the complicated equations, the time for one run (10 ms) ranged from 10–30 min depending on the time step. The equations were solved with the Diffpack program (23), running on a Linux operating system.

Taken together, the simulation results show that to reproduce the experimental data, the diffusion rate in the fuzzy space must be in the range of four orders of magnitude lower than in water. In addition, provided a Na^+ channel is present in the dyad close to an NCX molecule, the trigger Ca^{2+} from the reversal of the NCX will precede the Ca^{2+} from the LTCCs in reaching the RyRs. Thus, NCX is important for CICR. With a normal operating NCX, the SR Ca^{2+} release is up to 5 ms faster compared to a situation where the reverse NCX is not contributing to trigger Ca^{2+}. Hence, both the experimental and mathematical results clearly indicate the presence of a fuzzy space with restricted diffusion and an important role for local Na^+ provided by I_{Na} in reversing the NCX.

The authors gratefully acknowledge Morten Eriksen and Carsten Lund for animal care and Fredrik Swift for isolation of cardiomyocytes.

This study was supported by grants from the Research Council of Norway and the Anders Jahres Fund for Promotion of Science and Research Forum, Ullevaal University Hospital.

REFERENCES

1. Lederer, W. J., E. Niggli, and R. W. Hadley. 1990. Sodium-calcium exchange in excitable cells: fuzzy space. *Science*. 248:283.
2. Carmeliet, E. 1992. A fuzzy subsarcolemmal space for intracellular Na^+ in cardiac cells? *Cardiovasc. Res.* 26:433–442.
3. Cheng, H., W. J. Lederer, and M. B. Cannell. 1993. Calcium sparks: elementary events underlying excitation-contraction coupling in heart muscle. *Science*. 262:740–744.
4. Thomas, M. J., I. Sjaastad, K. Andersen, P. J. Helm, J. A. Wasserstrom, O. M. Sejersted, and O. P. Ottersen. 2003. Localization and function of the Na^+/Ca^{2+} exchanger in normal and detubulated rat cardiomyocytes. *J. Mol. Cell. Cardiol.* 35:1325–1337.
5. Hilgemann, D. W. 2004. New insights into the molecular and cellular working of the cardiac Na^+/Ca^{2+} exchanger. *Am. J. Physiol. Cell Physiol.* 287:C1167–C1172.
6. Sipido, K. R., M. Maes, and F. V. de Werf. 1997. Low efficiency of Ca^{2+} entry through the Na^+-Ca^{2+} exchanger as trigger for Ca^{2+} release from the sarcoplasmic reticulum. a comparison between L-type Ca^{2+} current and reverse-mode Na^+-Ca^{2+} exchange. *Circ. Res.* 81:1034–1044.
7. Vites, A. M., and J. A. Wasserstrom. 1996. Fast sodium influx provides an initial step to trigger contractions in cat ventricle. *Am. J. Physiol.* 40:H674–H686.
8. Litwin, S., O. Kohomoto, A. J. Levi, K. W. Spitzer, and J. H. Bridge. 1996. Evidence that reverse Na/Ca exchange can trigger SR calcium release. *Ann. N. Y. Acad. Sci.* 779:451–463.
9. Sham, J. S., L. Cleemann, and M. Morad. 1992. Gating of the cardiac Ca^{2+} release channel: The role of Na^+ current and Na^+/Ca^{2+} exchange. *Science*. 255:850–853.
10. Henderson, S. A., J. I. Goldhaber, J. M. So, T. Han, C. Motter, A. Ngo, C. Chantawansiri, M. R. Ritter, M. Friedlander, D. A. Nicoll, J. S. Frank, M. C. Jordan, K. P. Roos, R. S. Ross, and K. D. Philipson. 2004. Functional adult myocardium in the absence of Na^+/Ca^{2+} exchange: cardiac-specific knockout of NCX1. *Circ. Res.* 95:604–611.
11. Reuter, H., T. Han, C. Motter, K. D. Philipsson, and J. I. Goldhaber. 2003. Mice overexpressing the cardiac sodium-calcium exchanger: defects in excitation-contraction coupling. *J. Physiol.* 554:779–789.
12. Leblanc, N., and J. R. Hume. 1990. Sodium current-induced release of calcium from cardiac sarcoplasmic reticulum. *Science*. 248:372–376.
13. Wasserstrom, J. A., and A. M. Vites. 1996. The role of Na^+/Ca^{2+} exchange in activation of excitation-contraction coupling in rat ventricular myocytes. *J. Physiol.* 493:529–542.
14. Weber, C. R., V. Piacentino, K. S. Ginsburg, S. R. Houser, and D. M. Bers. 2002. Na^+/Ca^{2+} exchange current and submembrane $[Ca^{2+}]$ during the cardiac action potential. *Circ. Res.* 90:182–189.
15. Weber, C. R., K. S. Ginsberg, and D. M. Bers. 2003. Cardiac submembrane $[Na^+]$ transients sensed by Na^+/Ca^{2+} exchange current. *Circ. Res.* 92:950–952.
16. Winslow, R. L., J. Rice, S. Jafri, E. Marban, and B. O'Rourke. 1999. Mechanisms of altered excitation-contraction coupling in canine tachycardia-induced heart failure, II, model studies. *Circ. Res.* 84: 571–586.
17. Snyder, S. M., B. M. Palmer, and R. L. Moore. 2000. A mathematical model of cardiocyte Ca^{2+} dynamics with a novel representation of sarcoplasmic reticular Ca^{2+} control. *Biophys. J.* 79:94–115.
18. Pandit, S. V., R. B. Clark, W. R. Giles, and S. S. Demir. 2001. A mathematical model of action potential heterogeneity in adult rat left ventricular myocytes. *Biophys. J.* 81:3029–3051.
19. Sobie, E. A., K. W. Dilly, J. dos Santos Cruz, W. J. Lederer, and M. Jafri. 2002. Termination of cardiac Ca^{2+} sparks: An investigative mathematical model of calcium- induced calcium release. *Biophys. J.* 83:59–78.
20. Shannon, T. R., F. Wang, J. Puglisi, C. Weber, and D. M. Bers. 2004. A mathematical treatment of integrated Ca dynamics within the ventricular myocyte. *Biophys. J.* 87:3351–3371.

21. Despa, S., J. Kockskämper, L. A. Blatter, and D. M. Bers. 2004. Na/K pump-induced $[Na]_i$ gradients in rat ventricular myocytes measured with two-photon microscopy. *Biophys. J.* 87:1360–1368.
22. Langer, G. A., and A. Peskoff. 1996. Calcium concentration and movement in the diadic cleft space of the cardiac ventricular cell. *Biophys. J.* 70:1169–1182.
23. Langtangen, H. P. 2003. Computational Partial Differential Equations—Numerical Methods and Diffpack Programming, Vol. 2. Springer-Verlag, Berlin, Heidelberg.
24. Guatiomosim, S., K. Dilly, L. F. Santana, M. S. Jafri, E. A. Sobie, and W. J. Lederer. 2002. Local Ca^{2+} signaling and EC coupling in heart: Ca^{2+} sparks and the regulation of the $[Ca^{2+}]_i$ transient. *J. Mol. Cell. Cardiol.* 34:941–950.
25. Forbes, M. S., and E. E. V. Niel. 1988. Membrane systems of guinea pig myocardium: ultrastructure and morphometric studies. *Anat. Rec.* 222:362–379.
26. Amsellem, J., R. Delorme, C. Souchier, and C. Ojeda. 1995. Transverse-axial tubular system in guinea pig ventricular cardiomyocyte: 3D reconstruction, quantification and its possible role in K^+ accumulation-depletion phenomenon in single cells. *Biol. Cell.* 85:43–54.
27. Nakamura, S., J. Asai, and K. Hama. 1986. The transverse tubular system of rat myocardium: its morphology and morphometry in the developing and adult animal. *Anat. Embryol. (Berl.).* 173:307–315.
28. Ogata, T., and Y. Yamasaki. 1990. High-resolution scanning electron microscopic studies on the three-dimensional structure of the transverse-axial tubular system, sarcoplasmic reticulum and intercalated disc of the rat myocardium. *Anat. Rec.* 228:277–287.
29. Franzini-Armstrong, C., F. Protasi, and V. Ramesh. 1999. Shape, size, and distribution of Ca^{2+} release units and couplons in skeletal and cardiac muscles. *Biophys. J.* 77:1528–1539.
30. Soeller, C., and M. B. Cannell. 1999. Examination of the transverse tubular system in living cardiac rat myocytes by 2-photon microscopy and digital image-processing techniques. *Circ. Res.* 84:266–275.
31. Forbes, M. S., and N. Sperelakis. 1977. Myocardial couplings: their structural variations in the mouse. *J. Ultrastruct. Res.* 58:50–65.
32. Zhang, L., C. Franzini-Armstrong, V. Ramesh, and L. R. Jones. 2001. Structural alterations in cardiac calcium release units resulting from overexpression of junctin. *J. Mol. Cell. Cardiol.* 33:233–247.
33. Sun, X. H., F. Protasi, M. Takahashi, H. Takeshima, D. G. Ferguson, and C. Franzini-Armstrong. 1995. Molecular architecture of membranes involved in excitation-contraction coupling of cardiac muscle. *J. Cell Biol.* 129:659–671.
34. Wagenknecht, T., C. E. Hsieh, B. K. Rath, S. Fleischer, and M. Marko. 2002. Electron tomography of frozen-hydrated isolated triad junctions. *Biophys. J.* 83:2491–2501.
35. Radermacher, M., V. Rao, R. Grassucci, J. Frank, A. P. Timerman, S. Fleischer, and T. Wagenknecht. 1994. Cryo-electron microscopy and three-dimensional reconstruction of the calcium release channel/ryanodine receptor from skeletal muscle. J. *Cell Biol.* 127:411–423.
36. Yin, C. C., and F. A. Lai. 2000. Intrinsic lattice formation by the ryanodine receptor calcium-release channel. *Nat. Cell Biol.* 2:669–671.
37. Despa, S., F. Brette, C. H. Orchard, and D. M. Bers. 2003. Na^+/Ca^{2+} exchange and Na/K-ATPase function are equally concentrated in transverse tubules of rat ventricular myocytes. *Biophys. J.* 85:3388–3396.
38. Hilgemann, D. W., A. Collins, D. P. Cash, and G. A. Nagel. 1991. Cardiac Na^+/Ca^{2+} exchange system in giant membrane patches. *Ann. N. Y. Acad. Sci.* 639:126–139.
39. McCall, D. 1979. Cation exchange and glycoside binding in cultured rat heart cells. *Am. J. Physiol.* 236:c87–c95.
40. Yang, Z., C. Pascarel, D. S. Steele, K. Komukai, F. Brette, and C. H. Orchard. 2002. Na^+/Ca^{2+} exchange activity is localized in the t-tubules of rat ventricular myocytes. *Circ. Res.* 91:315–322.
41. Gathercole, D. V., D. J. Colling, J. N. Skeeper, Y. Tagagishi, A. J. Levi, and N. J. Severs. 2000. Immunogold-labeled L-type calcium channels are clustered in the surface plasma membrane overlying junctional sarcoplasmic reticulum in guinea-pig myocytes-implications for excitation-contraction coupling in cardiac muscle. *J. Mol. Cell. Cardiol.* 32:1981–1994.
42. Bers, D. M. 2001. Excitation-Contraction Coupling and Cardiac Contractile Force, Vol. 2. Kluwer Academic Publishers, Dordrecht, The Netherlands.
43. Satoh, H., K. S. Ginsberg, K. Qing, H. Tarada, H. Hayashi, and D. M. Bers. 2000. KB-R7943 block of Ca^{2+} influx via Na^+/Ca^{2+} exchange does not alter twitches or glycocides inotropy but prevents Ca^{2+} overload in rat ventricular myocytes. *Circulation.* 101:1441–1446.
44. Maier, S., R. Westenbroek, K. Schenkman, E. Feigl, T. Scheuer, and W. Catterall. 2002. An unexpected role for brain-type sodium channels in coupling of cell surface depolarization to contraction in the heart. *Proc. Natl. Acad. Sci. USA.* 99:4073–4078.
45. Brette, F., and C. Orchard. 2006. No apparent requirement for neuronal sodium channels in excitation-contraction coupling in rat ventricular myocytes. *Circ. Res.* 98:667–674.
46. Iwamoto, T., and S. Kita. 2004. Development and application of the Na^+/Ca^{2+} exchange inhibitors. *Mol. Cell. Biochem.* 259:157–161.
47. Viatchenko-Karpinski, S., D. Terentyev, L. Jenkins, L. Luther, and S. Györke. 2005. Synergistic interactions between Ca^{2+} entries through l-type Ca^{2+} channels and Na^+/Ca^{2+} exchanger in normal and failing heart. *J. Physiol.* 567:493–504.
48. Scriven, D., P. Dan, and E. Moore. 2000. Distribution of proteins implicated in excitation-contraction coupling in rat ventricular myocytes. *Biophys. J.* 79:2682–2691.
49. Semb, S. O., and O. M. Sejersted. 1996. Fuzzy space and control of Na^+, K^+-pump rate in heart and skeletal muscle. *Acta Physiol. Scand.* 156:213–225.
50. Fujioka, Y., S. Matsuoka, T. Ban, and A. Noma. 1998. Interaction of the Na^+-K^+ pump and the Na^+-Ca^{2+} exchange via $[Na_i^+]$ in a restricted space of guinea-pig ventricular cells. *J. Physiol.* 509: 457–470.
51. Verdonck, F., K. Mubagawa, and K. R. Sipido. 2004. $[Na^+]$ in the subsarcolemmal 'fuzzy' space and modulation of Ca_i^{2+} and contraction in cardiac myocytes. *Cell Calcium.* 35:603–612.
52. Wendt-Gallitelli, M. F., T. Voigt, and G. Isenberg. 1993. Microheterogeneity of subsarcolemmal sodium gradients. electron probe microanalysis in guinea-pig ventricular myocytes. *J. Physiol.* 472: 33–44.
53. Silverman, B. D. Z., A. Warley, J. I. A. Miller, A. F. James, and M. J. Shattock. 2003. Is there a transient rise in sub-sarcolemmal Na^+ and activation of Na^+/K^+ pump current following activation of I_{Na} in ventricular myocardium? *Cardiovasc. Res.* 57:1025–1034.
54. Kushmerick, M., and R. Podolsky. 1969. Ionic mobility in muscle cells. *Science.* 166:1297–1298.
55. Shannon, T. R., and D. M. Bers. 2004. Integrated Ca^{2+} management in cardiac myocytes. *Ann. N. Y. Acad. Sci.* 1015:28–38.
56. Vaughan-Jones, R., K. Spitzer, and P. Swietach. 2006. Spatial aspects of intracellular pH regulation in heart muscle. *Prog. Biophys. Mol. Biol.* 90:207–224.
57. Ellis, R. 2001. Macromolecular crowding: obvious but underappreciated. *Trends Biochem. Sci.* 26:597–604.
58. Spitzer, J., and B. Poolman. 2005. Electrochemical structure of the crowded cytoplasm. *Trends Biochem. Sci.* 30:536–541.
59. Luo, C. H., and Y. Rudy. 1994. A dynamic model of the cardiac ventricular action potential. *Circ. Res.* 74:336–349.
60. Barrere-Lemaire, S., C. Piot, F. L. Leclercq, J. Nargeot, and S. Richard. 2000. Facilitation of l-type calcium currents by diastolic depolarization in cardiac cells: impairment in heart failure. *Cardiovasc. Res.* 47: 336–349.
61. Bondarenko, V. E., G. C. L. Bett, and R. L. Rasmusson. 2004. A model of graded calcium release and l-type Ca^{2+} channel inactivation in cardiac muscle. *Am. J. Physiol. Heart Circ. Physiol.* 286:H1154–H1169.
62. Tanskanen, A. J., J. L. Greenstein, B. O'Rouke, and R. L. Winslow. 2005. The role of stochastic and modal gating of cardiac L-type Ca^{2+} channels on early after-depolarizations. *Biophys. J.* 88:85–95.

63. Weber, C. R., K. S. Ginsburg, K. D. Philipson, T. R. Shannon, and D. M. Bers. 2001. Allosteric regulation of Na^+/Ca^{2+} exchange current by cytosolic Ca in intact cardiac myocytes. *J. Gen. Physiol.* 117:119–131.

64. Sipido, K., M. Maes, and F. V. de Werf. 1997. Low efficiency of Ca^{2+} entry trough the Na^+-Ca^{2+} exchanger as trigger for Ca^{2+} release from the sarcoplasmic reticulum. *Circ. Res.* 81:1034–1044.

65. Lipp, P., and E. Niggli. 1994. Sodium current-induced calcium signals in isolated guinea-pig ventricular myocytes. *J. Physiol.* 474:439–446.

66. Kohomoto, O., A. Levi, and J. Bridge. 1994. Relation between reverse sodium-calcium exchange and sarcoplasmic reticulum calcium release in guinea pig ventricular cells. *Circ. Res.* 74:550–554.

67. Haworth, R., A. Goknur, and D. Hunter. 1991. Control of the Na-Ca exchanger in isolated heart cells. i. induction of Na-Ca exchange in sodium-loaded cells by intracellular calcium. *Circ. Res.* 69:1506–1513.

68. Litwin, S., J. Li, and J. Bridge. 1998. Na-Ca exchange and the trigger for sarcoplasmic reticulum Ca release: Studies in adult rabbit ventricular myocytes. *Biophys. J.* 75:359–371.

69. James, P. F., I. L. Grupp, G. Grupp, A. L. Woo, G. R. Askew, M. L. Croyle, R. A. Walsh, and J. B. Lingrel. 1999. Identification of a specific role for the Na/K-ATPase alpha 2 isoform as a regulator of calcium in the heart. *Mol. Cell.* 3:555–563.

70. Sande, J. B., I. Sjaastad, I. B. Hoen, J. Bokenes, T. Tonnessen, E. Holt, P. K. Lunde, and G. Christensen. 2002. Reduced level of serine^{16} phosphorylated phospholamban in the failing rat myocardium: a major contributor to reduced SERCA2 activity. *Cardiovasc. Res.* 53: 382–391.

71. Litwin, S. E., and J. H. B. Bridge. 1997. Enhanced Na^+/Ca^{2+} exchange in the infarcted heart. *Circ. Res.* 81:1083–1093.

72. Wasserstrom, J. A., E. Holt, I. Sjaastad, P. K. Lunde, A. Odegaard, and O. M. Sejersted. 2000. Altered E-C coupling in rat ventricular myocytes from failing hearts 6 wk after MI. *Am. J. Physiol. Heart Circ. Physiol.* 279:H798–H807.

73. Smith, G. D., J. E. Keizer, M. D. Sterm, J. Lederer, and H. Cheng. 1998. A simple numerical model of calcium spark formation and detection in cardiac myocytes. *Biophys. J.* 75:15–32.